Inorg. Chem. **2005**, *44*, 921–929

Hydrolytic Protein Cleavage Mediated by Unusual Mononuclear Copper(II) Complexes: X-ray Structures and Solution Studies

Mauricio C. B. de Oliveira,[†] Marciela Scarpellini,[‡] Ademir Neves,*[,‡] Hernán Terenzi,*[,†] Adailton J. Bortoluzzi,[‡] Bruno Szpoganics,[‡] Alessandra Greatti,[‡] Antônio S. Mangrich,[§] Emanuel M. de Souza,[||] Pablo M. Fernandez,[⊥] and Marcia R. Soares[#]

Laboratório de Expressão Gênica, Departamento de Bioquímica-CCB, Universidade Federal de Santa Catarina, 88040-900 Florianópolis, SC, Brazil, Laboratório de Bioinorgânica e Cristalografia-LABINC, Departamento de Química-CFM, Universidade Federal de Santa Catarina, 88040-900 Florianópolis, SC, Brazil, Departamento de Química, Universidade Federal do Paraná, 81531-970 Curitiba, PR, Brazil, Departamento de Bioquímica, Universidade Federal do Paraná, 81531-970 Curitiba, PR, Brazil, Unité de Biochimie Structurale, Institut Pasteur, 75724 Paris, France, and Laboratório de Espectrometria de Massas, Laboratório Nacional de Luz Sincrotron, 13083-100 Campinas, SP, Brazil

Received October 8, 2004

The crystal structures and redox and UV–vis/EPR spectroscopic properties of two new mononuclear copper(II) complexes, $[Cu(HL^1)Cl_2]$ (**1**) and $[Cu(L^1)Cl]$ (**2**), prepared through the reaction between copper(II) chloride and the ligand 2-[(bis(pyridylmethyl)amino)methyl]-4-methyl-6-formylphenol (HL^1) under distinct base conditions, are reported along with solution studies. Also, we demonstrate that these Cu^{II} complexes are able to cleave unactivated peptide bonds from bovine serum albumin (BSA) and the thermostable enzyme *Taq* DNA polymerase at micromolar concentration, under mild pH and temperature conditions. The cleavage activity seems to be specific with defined proteolytic fragments appearing after protein treatment. The location of the specific cleavage sites was tentatively assigned to solvent-accessible portions of the protein. These are two of the most active Cu(II) complexes described to date, since their cleavage activity is detected in minutes and evidence is here presented for a hydrolytic mechanism mediating protein cleavage by these complexes.

Introduction

The half-life of a peptide bond is estimated to be 7−600 years at neutral pH and ambient temperature, and these are one of the most stable chemical bonds in nature.[1−3] Typical biological catalysts such as carboxypeptidase A contains a zinc ion in their active sites, thus suggesting that small metal coordination complexes may play the role of a protease.[4] Because of the extreme stability of peptide bonds, their hydrolysis is often studied using activated amides. In fact there are few examples of the metal-promoted hydrolysis of peptide bonds in proteins; for a review, see refs 5−9 $Cu([9]aneN_3)Cl_2$ ([9]aneN$_3$ = 1,4,7-triazacyclononane) is an example of a metal complex able to hydrolyze the unactivated dipeptide glycyl−glycine and also the protein BSA, at near physiological pH.[10] This was the first complex able to cleave not only peptide bonds but also phosphodiester bonds,

* Authors to whom correspondence should be addressed. E-mail: ademir@qmc.ufsc.br (A.N.) Tel.: 55-48-331-9219 R226 (A.N.). Fax: 55-48-3319711 (A.N.).

[†] Departamento de Bioquímica-CCB, Universidade Federal de Santa Catarina.

[‡] Departamento de Química-CFM, Universidade Federal de Santa Catarina.

[§] Departamento de Química, Universidade Federal do Paraná.

[||] Departamento de Bioquímica, Universidade Federal do Paraná.

[⊥] Unité de Biochimie Structurale, Institut Pasteur.

[#] Laboratório de Espectrometria de Massas, Laboratório Nacional de Luz Sincrotron.

(1) Kahne, D.; Still, W. C. *J. Am. Chem. Soc.* **1988**, *110*, 7529−7534.
(2) Bryant, R. A. R.; Hansen, D. E. *J. Am. Chem. Soc.* **1996**, *118*, 5498−5499.
(3) Radzika, A.; Wolfenden, R. *J. Am. Chem. Soc.* **1996**, *118*, 6105−6109.
(4) Christianson, D. W.; Lipscomb, W. N. *Acc. Chem. Res.* **1989**, *22*, 62−69.
(5) Zhu, L.; Kostic, N. M. *Inorg. Chim. Acta* **2002**, *339*, 104−110.
(6) Polzin, G. M.; Burstyn, J. N. *Metal Ions in Biological Systems*; Marcel Dekker: New York, 2001; pp 104−143.
(7) Kaminskaia, N. V.; Kostic, N. M. *Inorg. Chem.* **2001**, *40*, 2368−2377.
(8) Hegg, E. L.; Burstyn, J. N. *Coordin. Chem. Rev.* **1998**, *173*, 133−165.
(9) Milovic, N. M.; Kostic, N. M. *J. Am. Chem. Soc.* **2002**, *124*, 4759−4769.

10.1021/ic0485864 CCC: $30.25
Published on Web 01/21/2005

Chart 1. Structure of Ligand HL^1

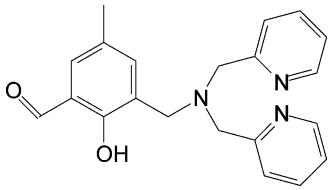

including DNA.[11−14] Zn(II) Obisdien (Obisdien = 1,4,7,13,16,19-hexaaza-10,22-dioxacyclotetracosane) was the second compound described to promote both glycyl−glycine and DNA phosphodiester bond cleavage.[15,16] A protein-cleaving catalyst, highly selective for myoglobin, has recently been synthesized, providing an important example of an artificial protease. This catalyst was designed by attaching the Cu(II) or Co(III) complex of cyclen to a binding site achieved by a combinatorial method using peptide nucleic acid monomers as building units.[17] The possible mechanisms of amide bond hydrolysis promoted by metals have been summarized by Polzin and Burstyn and involve electrophilic activation, metal hydroxide nucleophile attack, and general base or acid catalysis.[6] The use of chemical proteases as footprinting agents to map specific regions involved in protein−protein interactions has led to the identification of important contact sites and conformational changes in several proteins, such as cAMP-dependent protein kinase, cAMP receptor protein, and RNA polymerase.[18−20] Redox-active coordination complexes have also been used as peptide backbone cleavage agents.[21] Metal ions are also capable of interacting with proteins inducing conformational protein changes.[22−26]

In this paper we report the synthesis, X-ray structure, and physicochemical properties of two mononuclear copper(II)−chloro complexes containing the tripodal HL^1 ligand (Chart 1) and their activities toward the specific hydrolysis of BSA and *Taq* DNA polymerase.

Very recently, we published the synthesis and characterization of HL^1 as a suitable intermediate for the preparation of unsymmetrical dinucleating ligands.[27] While this work was nearing completion Reedijk et al.[28] reported the synthesis and X-ray analysis of the corresponding copper(II)−bromo complex containing HL^1, as an example of unexpected structure in which the carbonyl group of the ligand does not coordinate to the Cu^{II} and Mn^{II} ions. Complex **1** is demonstrated here to be one of the few metal complexes able to promote hydrolysis of BSA, in minutes at 50 °C and at micromolar concentration. As a comparison, Cu([9]aneN_3)-Cl_2 is capable to hydrolyze BSA at 50 °C after 48−96 h, at 0.5−1.5 mM.[10] Pd(II) complexes were defined as protein cleavage agents, active at millimolar concentration at 50 °C after several days of incubation period.[5]

Experimental Section

Abbreviations: HL^1, 2-[(bis(pyridylmethyl)amino)methyl]-4-methyl-6-formylphenol; (TBA)PF_6, tetrabutylammonium hexafluorophosphate; BSA, bovine serum albumin; Obisdien, 1,4,7,13,16,19-hexaaza-10,22-dioxacyclotetracosane; Cu([9]aneN_3)Cl_2, copper(II) 1,4,7-triazacyclononane dichloride; Hbpnp, (2-(bis(pyrid-2-ylmethyl)amino)methyl)-4-nitrophenol]; *Taq*, *Thermus aquaticus*; TRIS, Tris(hydroxymethyl)aminomethane; MOPS, 3-(*N*-morpholino)propanesulfonic acid; BTP, 1,3-bis((tris(hydroxymethyl)methyl)-amino)propane; AcOH/AcO^-, acetic acid/acetate buffer; Fc^+/Fc, ferrocenium/ferrocene; NHE, normal hydrogen electrode.

Materials. All chemicals and solvents used were reagent or spectroscopic grade purchased from commercial sources and used without further purification. BSA (electrophoretic purity) was obtained from Sigma. BTP, MOPS, and TRIS were obtained from USB. Plasmid pSG-NOR1 was a kindly donated by Prof. Mario Zakin, Inst. Pasteur, Paris, France. All solutions and buffers were prepared with Milli-Q water (Millipore).

Instrumentation. Infrared spectra were recorded on a Perkin-Elmer model 16PC spectrometer, in KBr pellets in the 4000−400 cm^{-1} range. Elemental analyses were performed on a Carlo Erba E-1110 instrument. Molar conductivities were measured on a Digimed CD-21 conductivimeter at 25 °C. UV−vis spectra were recorded on a Perkin-Elmer Lambda 19 spectrometer. Cyclic voltammograms were recorded with a Princeton Applied Research (PAR) 273 system at room temperature under argon atmosphere. These experiments were carried out by employing a standard three-component system: a glassy carbon working electrode; a platinum wire auxiliary electrode; an Ag/AgCl pseudoreference electrode constructed in our laboratory. To monitor the reference electrode, the ferrocenium/ferrocene couple was used.[29] EPR spectra were recorded on a Brucker ESP-300E spectrometer at room and liquid-N_2 temperature.

Ligand Synthesis of 2-[(Bis(pyridylmethyl)amino)methyl]-4-methyl-6-formylphenol (HL^1). The ligand HL^1 (Chart 1) was prepared according to the experimental procedure previously described.[27,30]

(10) Hegg, E. L.; Burstyn, J. N. *J. Am. Chem. Soc.* **1995**, *117*, 7015−7016.
(11) Burstyn, J. N.; Deal, K. A. *Inorg. Chem.* **1993**, *32*, 3585−3586.
(12) Deal, K. A.; Burstyn, J. N. *Inorg. Chem.* **1996**, *35*, 2792−2798.
(13) Deal, K. A.; Hengge, A. C.; Burstyn, J. N. *J. Am. Chem. Soc.* **1996**, *118*, 8, 1713−1718.
(14) Hegg, E. L.; Burstyn, J. N. *Inorg. Chem.* **1996**, *35*, 7474−7481.
(15) Luiz, M. T. B.; Szpoganicz, B.; Rizzoto, M.; Basallote, M. G.; Martell, A. E. *Inorg. Chim. Acta* **1999**, *287*, 134−141.
(16) Meier, M. M.; Karloh, P.; Terenzi, H.; Szpoganicz, B. *South. Braz. J. Chem.* **1999**, *7*, 11−23.
(17) Jeon, J. W.; Son, S. J.; Yoo, C. E.; Hong, I. S.; Suh, J. *Bioorg. Med. Chem.* **2003**, *11*, 2901−2910.
(18) Cheng, X.; Shaltiel, S.; Taylor, S. S. *Biochemistry* **1998**, *37*, 14005−14013.
(19) Baichoo, N.; Heyduk, T. *J. Mol. Biol.* **1999**, *290*, 37−48.
(20) Schmidt, B. D.; Meares, C. F. *Biochemistry* **2002**, *41*, 4186−4192.
(21) Gallagher, J.; Zelenko, O.; Walts, A. D.; Sigman, D. S. *Biochemistry* **1998**, *37*, 2096−2104.
(22) Shen, X.-C.; Liang, H.; Guo, J.-H.; Song, C.; He, X.-W.; Yuan, Y.-Z. *J. Inorg. Biochem.* **2003**, *95*, 124−130.
(23) Buranaprapuk, A.; Leach, S. P.; Kumar, C. V.; Bocarsly, J. R. *Biochim. Biophys. Acta* **1998**, *1387*, 309−316.
(24) Shrivastava, H. Y.; Nair, B. U. *Biochem. Biophys. Res. Commun.* **2000**, *270*, 749−754.
(25) Kocha, T.; Yamaguchi, M.; Ohtaki, H.; Fukuda, T.; Aoyagi, T. *Biochim. Biophys. Acta* **1997**, *1337*, 319−326.
(26) Rana, T. M.; Meares, C. F. *Proc. Natl. Acad. Sci. U.S.A.* **1991**, *88*, 10578−10582.
(27) Karsten, P.; Neves, A.; Bortoluzzi, A. J.; Drago, V.; Lanznaster, M. *Inorg. Chem.* **2002**, *41*, 4624−4626.
(28) Koval, A. I.; Huisman, M.; Stassen, A. F.; Gamez, P.; Lutz, M.; Spek, A. L.; Reedijk, J. *Eur. J. Inorg. Chem.* **2004**, 591−600.
(29) Gagne, R. R.; Koval, C. A.; Lisensky, G. C. *Inorg. Chem.* **1980**, *19*, 2854−2855.
(30) Neves, A.; Brito, N. A.; Drago, V.; Griesar, K.; Haase, W. *Inorg. Chim. Acta* **1995**, *237*, 131−135.

$[Cu(HL^1)(Cl)_2]\cdot 2H_2O$ (1). Complex **1** (Scheme 1) was obtained by mixing ethanolic solutions of the HL^1 ligand (0.35 g, 1 mmol, in 10 mL) and $CuCl_2\cdot 2H_2O$ (0.17 g, 1 mmol, in 10 mL), while stirring, at 50 °C for 15 min. After cooling of the solution to room temperature, a blue-green solid was formed, which was filtered off and washed with cold isopropyl alcohol and diethyl ether. This solid was recrystallized in aqueous solution in air, which resulted in blue crystals suitable for X-ray analysis. Yield: 0.39 g, 45%. Anal. Calcd for $CuC_{21}H_{21}N_3O_2Cl_2\cdot 2H_2O$: C, 48.70; H, 4.87; N, 8.11. Found: C, 48.79; H, 4.46; N, 8.10.

$[Cu(HL^1)Cl]\cdot H_2O$ (2). Complex **2** (Scheme 1) corresponds to the deprotonated form of **1**. Complex **2** was isolated as a green powder after treatment of **1** with a BTP buffer solution ($pH_{app} \sim 7.0$). Recrystallization of this material from a methanol/2-propanol (1:1) solution resulted in green crystals after leaving this solution to stand at room temperature for 1 week. Yield: 40%. Anal. Calcd for $CuC_{21}H_{20}N_3O_2Cl\cdot H_2O$: C, 54.43; H, 4.78; N, 9.07. Found: C, 54.33; H, 4.80; N, 9.48.

Potentiometric Equilibrium Studies. The potentiometric studies were carried out with a Micronal B375 pH meter fitted with a blue-glass electrode and a calomel reference electrodes calibrated to read $-\log [H^+]$ directly. The electrode was calibrated using the data obtained from a potentiometric titration of a known volume of a standard 0.100 mol·L^{-1} HCl solution with a standard 0.100 mol·L^{-1} KOH solution. The ionic strength of the HCl solution was maintained at 0.100 mol·L^{-1} by addition of KCl. Measurements were carried out in a thermostated cell containing a solution of the complex (0.05 mol/50 mL) with ionic strength adjusted to 0.100 mol·L^{-1} by addition of KCl, at 25.00 ± 0.05 °C. The experiments were performed under argon to eliminate the presence of atmospheric CO_2. Samples were titrated by addition of fixed volumes of a standard CO_2-free KOH solution (0.100 mol·L^{-1}). Computations were carried out with the BEST program, and species diagrams were obtained with SPE and SPEPLOT programs.[31]

Single-Crystal X-ray Structure Determination. A crystal of each sample was selected and fixed at the end of a glass fiber for X-ray analysis. The intensity data for complexes **1** and **2** were collected with an Enraf-Nonius CAD4 diffractometer, at room temperature, with graphite-monochromated Mo Kα radiation. The unit cell parameters were determined from the setting angles of 25 centered reflections. All data were corrected for Lorentz and polarization effects. An empirical absorption correction based on the azimuthal scans of 7 appropriate reflections was also applied to the collected intensities through the PLATON program.[32a] The structure was solved by direct methods and refined by full-matrix least-squares methods using the SIR97[32b] and SHELXL97[32c] programs, respectively. All non-hydrogen atoms were refined anisotropically. H atoms attached to C atoms were placed at their idealized positions, with C−H distances and U_{eq} values taken from the default settings of the refinement program. For complex **1**, the H atoms of the phenol group and one water molecule were found from a difference Fourier map, and these atoms were treated using a riding model. The second water molecule of crystallization is disordered over two alternative positions, with 0.55 and 0.45 site occupancy, and its H atoms were not found. For complex **2**, the H atoms of the water molecule of crystallization were found from a Fourier map and also treated with a riding model. The figures of the molecular structures were produced with the ZORTEP program.[32d] Further crystal structure and refinement data for complexes **1** and **2** are summarized in Table 1.

Table 1. Summary of Crystallographic Data for Complexes **1** and **2**

	complex **1**	complex **2**
formula	$C_{21}H_{25}Cl_2CuN_3O_4$	$C_{21}H_{22}ClCuN_3O_3$
fw	517.88	463.41
T (K)	293(2)	293(2)
λ (Å)	0.710 73	0.710 73
cryst system	triclinic	monoclinic
space group	$P\bar{1}$	$P2_1/n$
a (Å)	7.807(2)	8.311(2)
b (Å)	8.817(2)	12.782(3)
c (Å)	17.929(4)	19.824(4)
α (deg)	103.89(3)	
β (deg)	90.74(3)	100.72(3)
γ (deg)	110.61(3)	
V (Å^3)	1115.0(4)	2069.2(8)
Z	2	4
ρ_{calc} (g·cm^{-3})	1.543	1.488
μ (mm^{-1})	1.252	1.212
F(000)	534	956
reflcns	4784	3941
unique reflns	3947 ($R_{int} = 0.0163$)	3669 ($R_{int} = 0.0292$)
params	290	263
GOF (F^2)	1.067	1.010
$R(F)^a$ ($I > 2\sigma(I)$)	0.0311	0.0338
$R_w(F^2)^b$ (all data)	0.0857	0.0914

^{a} $R(F) = \sum||F_o| - |F_c||/\sum|F_o|$. ^{b} $R_w(F^2) = \{\sum[w(F_o^2 - F_c^2)^2/\sum[w(F_o^2)^2]\}^{1/2}$.

***Taq* DNA Polymerase Inhibition Assay.** Amplification of a target DNA was performed using pSG-NOR1 (2 ng/μL) as the DNA matrix, a plasmid containing the coding sequence of the nor-1 orphan nuclear receptor, primers H_4/H_5 (0.24 μM; primers directed toward a 899 bp fragment of Nor-1), $MgCl_2$ (3 mM), dNTPs (200 μM), buffer (50 mM KCl, 10 mM Tris-Cl, pH 8.8), and *Taq* DNA polymerase (2.5 U, ∼100 ng of protein), in a final volume of 20 μL. The amplification conditions were as follows: melting (45 s, 94 °C); primer annealing (30 s, 45 °C); extension (90 s, 72 °C). These steps were repeated 30 times, and a final 10 min extension was added at the end of this process. The products were analyzed by 0.8% agarose gel electrophoresis.[33] For the *Taq* DNA polymerase cleavage assay the reaction conditions were the same as those for the inhibition assay, with the exception of plasmid, primers, and dNTP.

BSA Cleavage Assay. BSA was incubated in 50 mM Tris-HCl at pH 8.9, AcOH/AcO^- pH 4.7, or MOPS pH 7.2, with different concentrations of complex **1**, at several incubation times and temperatures. At the end of the incubation period, an aliquot was mixed with loading buffer 2X (100 mM Tris-HCl pH 6.8, 7% SDS, 20% glycerol, 2% β-mercaptoethanol, and 0.01% bromophenol blue) and maintained at −20 °C. The samples were analyzed by SDS−PAGE.

Anaerobic Reactions. Samples were prepared through modifications in the experimental procedure previously described by Scarpellini et al.[34] for DNA cleavage. Briefly, BSA (5 μM) was incubated with, or without, complex **1**, $[Fe(EDTA)]^{2-}$/DTT, or

(31) Martell, A. E.; Motekaitis, R. J. *Determination and Use of Stability Constants*; VHC Publishers: Weinheim, Germany, 1992.

(32) (a) Spek, A. L. *Acta Crystallogr., Sect. A* **1990**, *36*, C34. (b) Altomare A.; Burla M. C.; Camalli, M.; Cascarano, G. L.; Giacovazzo, C.; Guagliardi, A.; Moliterni, A. G. G.; Polidori, G.; Spagna, R. *J. Appl. Crystallogr.* **1999**, *32*, 115−119. (c) Sheldrick, G. M. *SHELXL 97, Program for the Refinement of Crystal Structures*; University of Göttingen: Göttingen, Germany, 1997. (d) Zolnai, L. *ZORTEP. An interactive ORTEP program*; University of Heidelberg: Heidelberg, Germany, 1997.

(33) Neves, A.; Terenzi, H.; Horner, R.; Horn Jr., A.; Szpoganicz, B.; Sugai, J. *Inorg. Chem. Commun.* **2001**, *4*, 388−391.

(34) Scarpellini, M.; Neves, A.; Horner, R.; Bortoluzzi, A. J.; Szpoganicz, B.; Zucco, C.; Silva, R. A. N.; Drago, V.; Mangrich, A. S.; Ortiz, W. A.; Passos, A. C. W.; Oliveira, M. C. B.; Terenzi, H. *Inorg. Chem.* **2003**, *42*, 8353−8365.

Scheme 1. Structures of the Complexes

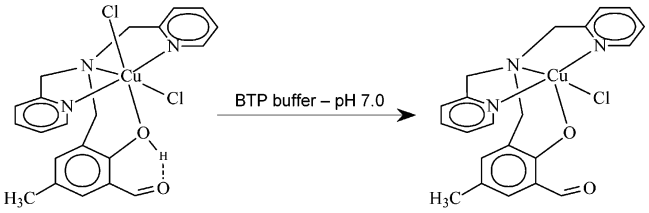

1 **2**

Table 2. Selected Bond Lengths (Å) and Angles (deg) for Complex **1**

Cu1−N12	2.014(2)	N1−Cu1−Cl2	165.48(6)
Cu1−N32	2.018(2)	N12−Cu1−Cl1	94.02(7)
Cu1−N1	2.068(2)	N32−Cu1−Cl1	89.39(7)
Cu1−Cl2	2.2628(10)	N1−Cu1−Cl1	94.06(6)
Cu1−Cl1	2.6047(10)	Cl2−Cu1−Cl1	100.46(3)
Cu1−O1	2.822(2)	N12−Cu1−O1	80.93(7)
N12−Cu1−N32	162.26(8)	N32−Cu1−O1	95.10(7)
N12−Cu1−N1	81.16(8)	N1−Cu1−O1	84.11(7)
N32−Cu1−N1	81.24(8)	Cl2−Cu1−O1	81.41(5)
N12−Cu1−Cl2	97.62(7)	Cl1−Cu1−O1	174.83(4)
N32−Cu1−Cl2	98.87(7)	C32−O1−Cu1	94.98(14)

DMSO in 50 mM MOPS buffer pH 7.0 at 50 °C for 6 h. After the incubation period, reactions were stopped as in the aerobic experiments. All other conditions and procedures were the same as those for aerobic reactions.

Protein Electrophoresis (SDS−PAGE). Protein samples were submitted to a discontinuous SDS−PAGE (4% acrylamide for stacking gel and 10% acrylamide for separation gel)[35] in a Gibco BRL vertical gel electrophoresis apparatus (model V15.17), carrying out the experiments at 15 mA (stacking) and 25 mA (separation). The gels were either Coomassie blue or silver stained, their images were acquired using a photodocumentation system, and protein bands were quantified using LabWorks Software v4.0 (UVP, Inc.).

Results and Discussion

Mononuclear Copper(II) Complex Containing the Tripodal HL^1 Ligand. In this work we present the synthesis and physicochemical properties of two new mononuclear copper(II) complexes containing the tripodal HL^1 ligand (complexes **1** and **2**, Scheme 1) and their activities toward the specific hydrolysis of BSA and *Taq* DNA polymerase. The infrared spectra of complexes **1** and **2** show typical vibrations of the skeletal ligand, in which the ν(C═O) of the formyl group is observed around 1650 cm^{-1}. As the out of plane δ(O−H$_{phenol}$) vibration (1373 cm^{-1} for **1**) is not observed in the spectrum of complex **2**, it is likely that complex **2** is the deprotonated form of complex **1**.

X-ray Structural Characterization. Complex **1** crystallizes as light blue crystals that belong to the triclinic crystal system, space group $P\bar{1}$. The crystallographic data and the main distances and angles for complex **1** are presented in Tables 1 and 2, respectively. X-ray analysis shows that the Cu^{II} center in complex **1** (Figure 1) is in a N_3OCl_2 coordination moiety of distorted octahedral geometry. Three nitrogen atoms from the HL^1 ligand and one chloride anion comprise the equatorial plane, in such a way that the pyridine nitrogen atoms, N12 and N32, are positioned trans to each other. The chloride anion Cl1 and the phenol oxygen O1 are coordinated at the axial positions and complete the coordination sphere of the metal center. The long distance (Cu1−O1 = 2.822(2) Å) observed for the coordination of the phenol group suggests that it is protonated. In fact, a phenol hydrogen was found in the Fourier-difference electronic density map and an intramolecular hydrogen bond is observed between it and the carbonyl oxygen O2: O1−H1···O2 = 1.67 Å. This phenol coordination mode has also been reported for mono-[36−38] and dinuclear[39−41] Cu^{II} complexes, in which the Cu^{II}−OH bond distances range from 2.268 Å for the [Cu(bpnp)Cl] complex[41] to 2.932(2) Å for [Cu(HL^1)Br$_2$].[28] To the best of our knowledge the values observed for the Cu−OH$_{phenol}$ distance in **1** and in the corresponding bromo complex are the longest reported until now and are therefore best regarded as being only a semicoordination of the oxygen atom to the Cu^{II} ion. The Cu−N$_{pyridine}$ bond distances in complex **1** [average = Cu−N = 2.016(2) Å] are similar to those observed in the [Cu(HL^1)Br$_2$] complex (2.020 Å) and are also in the range of Cu−N$_{pyridine}$ distances determined for other mononuclear copper(II) complexes[42] in which the pyridine rings are also positioned trans to each other. By contrast, the Cu−Cl bond distances (Cu1−Cl1 =

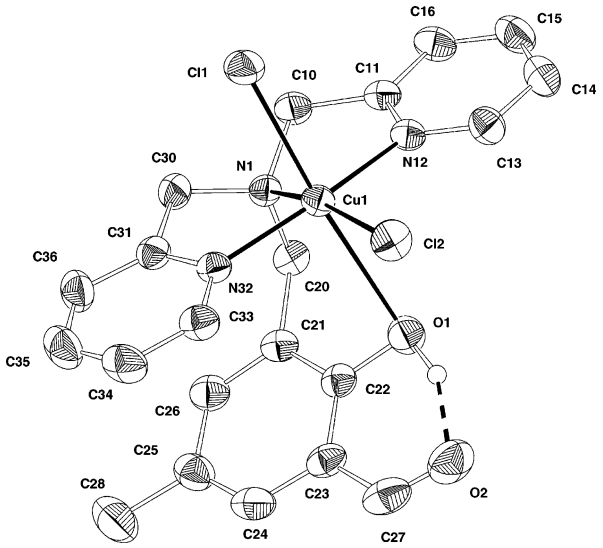

Figure 1. View of the complex [Cu(HL^1)Cl$_2$]·2H$_2$O (**1**) with atom-labeling scheme and ellipsoids at 40% probability.

(35) Laemmli, U. K. *Nature* **1970**, *227*, 680−685.

(36) (a) Neves, A.; Vencato, I.; Verani, C. N. *Acta Crystallogr., Sect. C* **1996**, *C52*, 1648−1651. (b) Neves, A.; Verani, C. N.; de Brito, M. A.; Vencato, I.; Mangrich, A. S.; Oliva, G.; Souza, D. D. H. F.; Batista, A. A. *Inorg. Chim. Acta* **1999**, *290*, 207−212.

(37) Masuda, H.; Odani, A.; Yamauchi, O. *Inorg. Chem.* **1989**, *28*, 624−625.

(38) Rajendran, U.; Viswanathan, R.; Palaniandavar, M.; Lakshminarayanan, M. *J. Chem. Soc., Dalton Trans.* **1992**, 3563−3564.

(39) Neves, A.; Rossi, L. M.; Horn, A., Jr.; Vencato, I.; Bortoluzzi, A. J.; Zucco, C.; Mangrich, A. S. *Inorg. Chem. Commun.* **1999**, *8*, 334−337.

(40) Neves, A.; Rossi, L. M.; Vencato, I.; Drago, V.; Haase, W.; Werner, R. *Inorg. Chim. Acta* **1998**, *281*, 111−115.

(41) (a) Vaidyanathan, M.; Viswanathan, R.; Palaniandavar, M. Balasubramanian, T.; Prabhaharan, P.; Muthiah, T. P. *Inorg. Chem.* **1998**, *37*, 6418−6427. (b) Uma, R.; Viswanathan, R.; Palaniandavar, M.; Lakshminarayanan, M. J. *J. Chem. Soc., Dalton Trans.* **1994**, 1219−1226.

(42) Karlin, K. D.; Hayes, J. C.; Juen, S., Hutchinson, J. P.; Zubieta, J. *Inorg. Chem.* **1982**, *21*, 4106−4108.

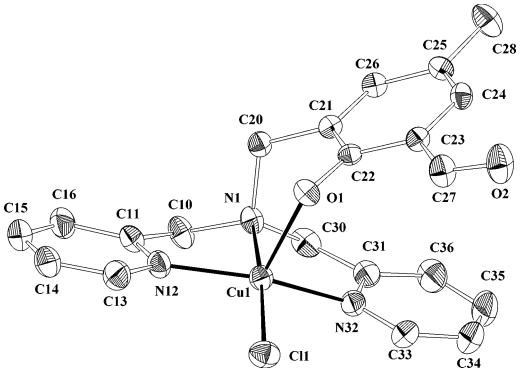

Figure 2. View of the complex $[Cu(L^1)Cl]\cdot H_2O$ (**2**) with atom-labeling scheme and ellipsoids at 40% probability.

Table 3. Selected Bond Lengths (Å) and Angles (deg) for Complex **2**

Cu1−N12	2.001(2)	N12−Cu1−O1	107.80(10)
Cu1−N32	2.013(3)	N32−Cu1−O1	90.60(9)
Cu1−N1	2.070(2)	N1−Cu1−O1	92.45(9)
Cu1−O1	2.130(2)	N12−Cu1−Cl1	95.63(8)
Cu1−Cl1	2.2784(10)	N32−Cu1−Cl1	96.91(9)
N12−Cu1−N32	156.46(11)	N1−Cu1−Cl1	171.52(7)
N12−Cu1−N1	81.85(10)	O1−Cu1−Cl1	96.03(6)
N32−Cu1−N1	82.84(11)	C22−O1−Cu1	116.10(17)

2.6047(10) and Cu1−Cl2 = 2.2628(10) Å) are the longest of the coordination sphere and lie in the range of values reported for other similar complexes.[12,42,43] However, as expected, these bond lengths are ∼0.12 Å shorter than the corresponding Cu−Br distances detected in the $[Cu(HL^1)Br_2]$ complex.[28]

Complex **2** crystallizes in such a way that the crystals are olive-green or red depending on the incident light angle. These crystals belong to the monoclinic crystal system, space group $P2_1/n$; the crystallographic data as well as the main distances and angles are presented in Tables 1 and 3, respectively. In the structure of **2** (Figure 2), the Cu^{II} ion lies in a square pyramidal geometry ($\tau = 0.14$)[44] with the L^1 donor atoms occupying the same positions observed for complex **1**. All the Cu^{II}−N bond distances (Table 3) are similar to those of complex **1**. The primary difference observed between complexes **1** and **2** is a shortening of the Cu1−O1 bond distance from 2.822(2) Å in complex **1** to 2.130(2) Å in complex **2** indicative of coordination by a deprotonated phenol group.

Potentiometric Equilibrium Determinations. As *cis*-dihalo Cu^{II} complexes generate *cis*-diaquo Cu^{II} complexes in aqueous solution, potentiometric titrations of complex **1** were carried out that revealed two titratable protons with pK_a values of 5.75 and 9.23 (Figure 3). The pK_{a1} at 5.75 was attributed to the deprotonation of the phenol-bound ligand yielding its deprotonated form (complex **2**) containing the $Cu-O_{phenolate}$ moiety. This assignment is based on

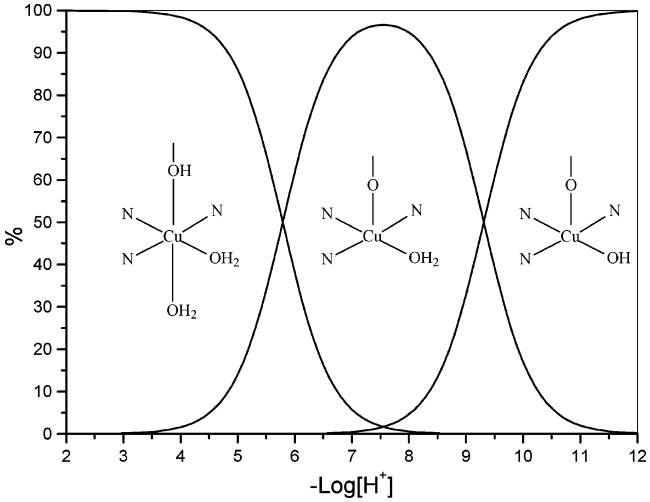

Figure 3. Species distribution curves for complex **1** as a function of −log $[H^+]$, where pK_{a1} = 5.75 and pK_{a2} = 9.23.

Table 4. Absorption Spectral Data for Complexes **1** and **2**

complex	medium	λ_{max} (nm)/(ϵ/mol·L^{-1}·cm^{-1})
1[a]	solid	793/368
1[b]	CH_3CN	720 (146)
2[a]	solid	736/427
2[b]	CH_3CN	731 (138), 498 (500), 393 (5500)
1[c]	H_2O/pH = 3.5	664 (72)
	H_2O/pH = 7.5	680 (74), 393 (5407)
	H_2O/pH = 10.8	670 (73), 394 (5270)

[a] Solid sample in MgO. [b] [**1**] = 1.0 × 10^{-3} mol·L^{-1}, [**2**] = 1.0 × 10^{-3} mol·L^{-1}. [c] [**1**] = 5 × 10^{-3} mol·L^{-1}; pH adjusted with HCl and KOH solutions.

Table 5. EPR Measurement Conditions and Results for Complex **1**

medium	$g_\perp$	$g_\parallel$	$10^4A_\parallel$ (cm^{-1})	$g_\parallel/A_\parallel$
solid (RT)[a]	2.078	2.180	100.0	218
solid (77 K)	2.100	2.175	100.0	217
ethanol/buffer (5.5)[b] (77 K)	2.065	2.260	180.0	126
ethanol/buffer (7.5)[c] (77 K)	2.065	2.250	182.0	124
ethanol/buffer (9.3)[d] (77 K)	2.060	2.250	180.0	125

[a] RT = room temperature. [b] MES buffer, pH = 5.5. [c] Trizma buffer, pH = 7.5. [d] CHES buffer, pH = 9.3.

electronic spectral changes which occur with increasing pH; complex **2** shows the appearance of a typical phenolate → Cu^{II} LMCT[37] around 400 nm (vide infra). The second pK_{a2} at 9.23 is likely related to a copper coordinated water molecule. This value is similar to those determined for other Cu^{II} complexes[34,43a] containing equatorially coordinated water molecules.

UV−Vis and EPR Spectroscopies. The UV−vis and EPR experimental conditions and results for complexes **1** and **2** are shown in Tables 4 and 5, respectively. The electronic spectrum of complex **1** in the solid-state (diffuse reflectance, Table 4) presents a typical tetragonally distorted octahedral feature[45] with a large d−d band centered at 793 nm in agreement with its structural analysis. However, when the spectrum is taken in acetonitrile solution, the position of this band shifts to 720 nm. A plausible explanation for this shift may be related to the exchange of the chloro ligands with

(43) (a) Young, M. J.; Wahnon, D.; Hynes, R. C.; Chin, J. *J. Am. Chem. Soc.* **1995**, *117*, 9441−9447. (b) Hegg, E. L.; Mortimore, S. H.; Cheung, C. L.; Huyett, J. E.; Powell, D. R.; Burstyn, J. N. *Inorg. Chem.* **1999**, *38*, 2961−2968. (c) Schwindinger, W. F.; Fawcett, T. G.; Lalancette, R. A.; Schugar, H. J.; Potenza, J. A. *Inorg. Chem.* **1980**, *19*, 1379−1381.

(44) Addison, A. W.; Rao, T. N.; Reedijk, J.; Vanrijn, J.; Verschoor, G. C. J. *J. Chem. Soc., Dalton Trans.* **1984**, 1349−1356.

(45) Lever, A. B. P. *Inorganic Electronic Spectroscopy*; Elsevier Science Publishers BV: Amsterdam, 1984; pp 553−572.

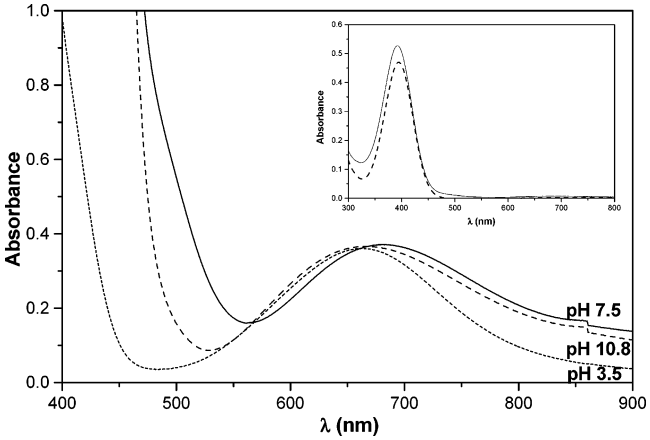

Figure 4. UV−vis spectra of **1** in aqueous solution at different pH values solution, [**1**] = 5×10^{-3} and 1×10^{-4} mol·L^{-1} (inset): (•••) pH 3.5; (---) pH 7.5; (—) pH 10.8.

CH_3CN molecules as observed for the $[Cu(HL^1)Br_2]$ complex.[28] Complex **2** also presents spectra in accordance with its structural analysis (Table 4). In the solid state two bands around 750 and 500 nm are observed, which are typical of square-pyramidal complexes.[38,45] In acetonitrile the spectrum of complex **2** displays, besides a broad band around 730 nm, a LMCT band at 393 nm ascribed as a phenolate → Cu^{II} transition.[38]

The UV−vis spectra of **1** (Table 4) were also recorded in aqueous solution at different pH values to confirm the protonation/deprotonation equilibria observed in the potentiometric titration experiments. Under acidic conditions (pH = 3.5), in the range 400−900 nm, the spectrum reveals only one d−d absorption band at 663 nm (Figure 4) which is significantly blue shifted when compared to the corresponding absorption (λ_{max} = 793 nm) of $[Cu(HL^1)Cl_2]$ (**1**) in the solid state. This suggests that the chloride ligands are being replaced by water molecules. When the pH of the aqueous solution of **1** is raised to 7.5, the LMCT band at 392 nm, ascribed as a phenolate → Cu^{II} transition, is observed (inset of Figure 4), while λ_{max} of the d−d transition is only slightly affected. This result clearly indicates that deprotonation of the coordinated phenol group is taking place, in full agreement with the potentiometric titration data (pK_{a1} = 5.75) and the spectrum of **2** which shows λ_{max} = 393 nm under identical experimental conditions. Finally, at pH = 10.8, as expected, the charge transfer band remains essentially unchanged (Figure 4, inset) while the d−d band is displaced to higher energies (λ_{max} = 670 nm, Figure 4), in agreement with deprotonation of a bound water molecule (pK_{a2} = 9.23) as determined through potentiometry.

EPR spectra of complex **1** were recorded in different media, and simulation parameters are presented in Table 5. In the solid state, spectra recorded at room and liquid-N_2 temperatures are in agreement with the distorted octahedral geometry observed in the X-ray analysis. Both spectra show an axial symmetry ($g_{\|} > g_{\perp}$) with a $d_{x^2-y^2}$ ground state. The spectra of complex **1** recorded in ethanol/buffer solutions at pH values of 7.5 and 9.3 show (Table 5 and Figure S1) a decrease in the $g_{\|}$ and a slight increase in the $A_{\|}$ value. This behavior has been interpreted as an increase in the strength of the metal−ligand covalent bond[46] in agreement with deprotonation of the phenol group.

Table 6. CV Results (in V) for Complexes **1** and **2** in Different Media[a]

complex	medium	E_{pc}	E_{pa}	$E_{1/2}$
1	CH_2Cl_2[b]	−0.671	−0.472	−0.572
	CH_3OH[b]	−0.639	−0.519	−0.579
	H_2O (pH = 3.5)[c]	−0.143		
	H_2O (pH = 7.5)[c]	−0.255		
	H_2O (pH = 10.8)[c]	−0.424	−0.292	−0.358
2	CH_3OH[b]	−0.829	−0.704	−0.767

[a] Reference electrode: Ag/AgCl. Auxiliary electrode: platinum. Working electrode: glassy carbon. [b] Supporting electrolyte 0.1 mol·L^{-1} (TBA)PF_6; ferrocene as internal standart; E values versus Fc^+/Fc. [c] Supporting electrolyte 0.1 mol·L^{-1} KCl; E values versus NHE.

Cyclic Voltammetry. Cyclic voltammograms (CVs) of complexes **1** and **2** were recorded in organic solvents, with (TBA)PF_6 as the supporting electrolyte. Results are summarized in Table 5, and typical voltammograms of **1** in CH_2Cl_2 at different scan rates are displayed in Figure S1. The experiments were carried out in dichloromethane to investigate the species containing coordinated chloride ligands; experiments in methanol were intended to give information on species with coordinated methanol molecules. The cyclic voltammograms of **1** in dichloromethane (Figure S2) exhibit a reversible wave at −0.57 V vs Fc^+/Fc attributed to the $Cu^{II} \rightarrow Cu^I$ redox process in the $[Cu^{II}(HL^1)Cl_2]$ species. In pure methanol, the same behavior is observed with a unique $Cu^{II} \rightarrow Cu^I$ redox process at −0.58 V vs Fc^+/Fc, which we also attribute to the Cu^{II}/Cu^I redox couple without changing the first coordination sphere of the $[Cu^{II}(HL^1)Cl_2]$ species (Figure S3). The cyclic voltammogram of complex **2** in pure methanol shows only one reversible process at −0.77 V vs Fc^+/Fc that corroborates with the coordination of the phenol in its deprotonated form.

As with the UV−vis experiments, cyclic voltammograms in aqueous solution, at different pH values, were recorded to identify the phenol/phenolate and aquo/hydroxo species in complexes **1** and **2**. In fact, these results agree very well with those obtained from UV−vis and potentiometric data. When the CV for **1** is recorded at pH = 3.5 (Table 6), a single irreversible redox process at −0.143 V vs NHE (Figure 5a) is observed, which we attribute to the $[Cu^{II}(HL^1)(OH_2)]^{2+} \leftrightarrow [Cu^I(HL^1)(OH_2)]^+$ redox couple. Under these experimental conditions the phenol group of HL^1 is expected to be coordinated in its protonated form as has been observed in the potentiometric titration as well as in the UV−vis studies of **1**. At pH = 7.5, the CV of **1** (Figure 5b) shows a cathodic shift of 112 mV suggesting that the coordinating phenol group becomes deprotonated thus lowering the Lewis acidity of the Cu^{II} center. The sharp oxidation peak during the reverse scan (E_{pa} = −0.065 and E_{pa} = −0.085 V vs NHE observed in the CVs a and b, respectively) is tentatively attributed to adsorption of the complex onto the electrode surface. Alternatively, deposit of copper(0) on the electrode surface can originate the typical features of a redissolution

(46) Auerbach, U.; Eckert, U.; Wieghardt, K.; Nuber, B.; Weiss, J. *Inorg. Chem.* **1990**, *29*, 938−944.

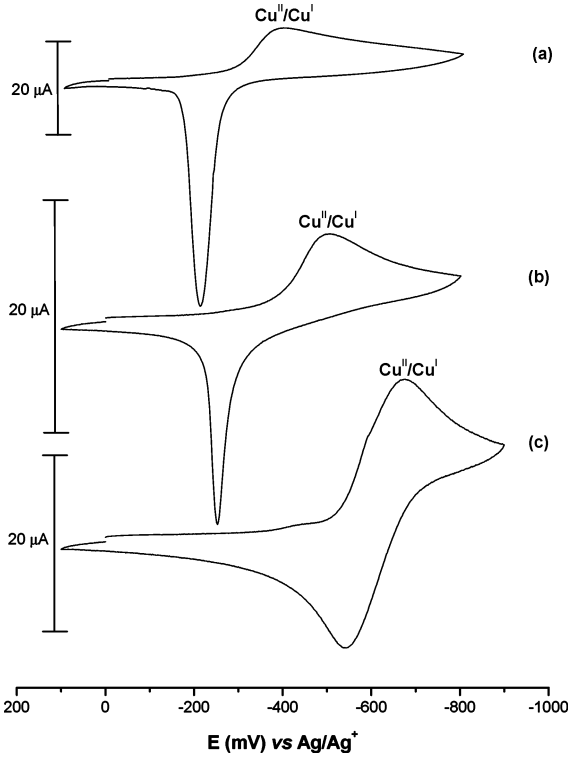

Figure 5. Cyclic voltammograms of complex **1** in aqueous solution (0.1 mol L^{-1} KCl supporting electrolyte, glassy carbon working electrode, platinum wire auxiliary electrode, Ag/AgCl reference eletrode; scan rate 25 mV·s^{-1}): (a) pH 3.5; (b) pH 7.5; (c) pH 10.8.

Scheme 2. Equilibria and Redox Reactions for **1** and **2** in Aqueous Solution

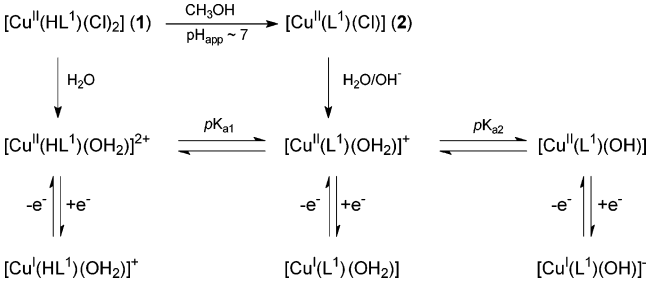

process during the reverse scan.[47] Finally, at pH = 10.8, the cyclic voltammogram of **1** (Figure 5c) becomes quasi-reversible with the reduction potential being displaced cathodically by 170 mV with respect to the potential at pH = 7.5 which could result from deprotonation of an equatorially copper coordinated water molecule in **1**. If one takes the potentiometric titration, the UV−vis, and the CV data together, the equilibria and redox reactions in Scheme 2 can be proposed.

***Taq* DNA Polymerase Inhibition and Cleavage.** *Taq* DNA polymerase, an enzyme used to amplify target DNA in polymerase chain reaction assays (PCR), is sensitive to complex **1** degradation activity. As observed in Figure 6, the level of enzyme cleavage increased with increasing complex **1** concentration, and as expected, enzyme activity also decreased with increasing complex **1** concentration. The activity of *Taq* DNA polymerase, assayed by a PCR technique (see Experimental Section), seemed to be slightly more sensitive to complex **1** than the corresponding degradation of the whole protein (compare Figure 6, sets A1 and A2 and the two curves in set B). This may occur due to targeting of complex **1** to the catalytic site of *Taq* DNA polymerase, since complex **1** is also capable of DNA binding and cleavage (not shown, manuscript in preparation) and thus may act in close proximity to the catalytic site of this DNA polymerase. Using a concentration of only 30 μM of complex **1** promoted 50% cleavage of *Taq* DNA polymerase, in a condition typical of a polymerase chain reaction (Figure 6). It is important to stress the fact that complex **1** is unable to cleave DNA under the conditions used in the PCR reaction, thus indicating that the 899 bp PCR product was not simply degraded by complex **1**.

BSA Cleavage Activity. The activity of complex **1** toward protein peptide bonds was assayed with bovine serum albumin (BSA) as described in the Experimental Section. The cleavage activity is strictly dependent on complex **1** concentration (Figure 7). The initial rate of BSA cleavage for each complex **1** concentration follows a pseudo-first-order saturation kinetics. As an example**,** with 150 μM of complex **1**, at pH 7.2 the BSA cleavage half-lives were estimated as 30 and 0.2 min at 50 and 70 °C, respectively. The activation energy (E_a), calculated at pH 7.2, was ~67 kJ/mol. These data demonstrate that complex **1** is one of the most active artificial proteases synthesized to date.[5,10]

The influence of pH (Figure 8) on the cleavage reaction was analyzed using BSA as the substrate. The pH also has an important effect on the activity of complex **1**. When complex **1** is under physiological pH conditions, its deprotonated form (complex **2**) containing the Cu−O$_{phenolate}$ moiety (pK_{a1} = 5.75) and an equatorially coordinated water molecule is generated. Apparently this is the most active species since a significant increase in the activity of BSA cleavage was observed. The effect of pH on complex **1** activity is demonstrated by saturation kinetics plots at different pH values, shown in Figure S4.

The BSA cleavage profile observed at higher BSA concentration (10 μM; Figure 9) is not a smear, thus prompting us to detect the fragmentation of BSA. We observed a BSA cleavage profile in the absence of complex **1**, mainly due to spontaneous cleavage sites present in BSA (see lanes 1, 5, and 9 in Figure 9). These spontaneous cleavage sites were identified as Asp susceptible residues exposed to mild acidic conditions.[5,48] However, when BSA was incubated with complex **1**, novel protein fragments were observed and most probably were due to complex **1** specific BSA structural targets (Figure 9). We hypothesize that the more exposed BSA secondary structures are prone to cleavage by complex **1**, as is the case with several proteins.[17−20] A model of the more exposed BSA secondary structure elements is depicted in Figure 10. In Table 7 we compare the fragmentation profile of BSA (Figure 9) with the proposed cleavage sites in BSA (Figure 10, amino acid

(47) Zurita, D.; Scheer, C.; Pierre, J.-L.; Saint-Aman, E. *J. Chem. Soc., Dalton Trans.* **1996**, 4331−4336.

(48) Anfinsen, C. B.; Edsall, J. T.; Richards, F. M. *Advances in Protein Chemistry*; Academic Press: New York, 1985; pp 161−245.

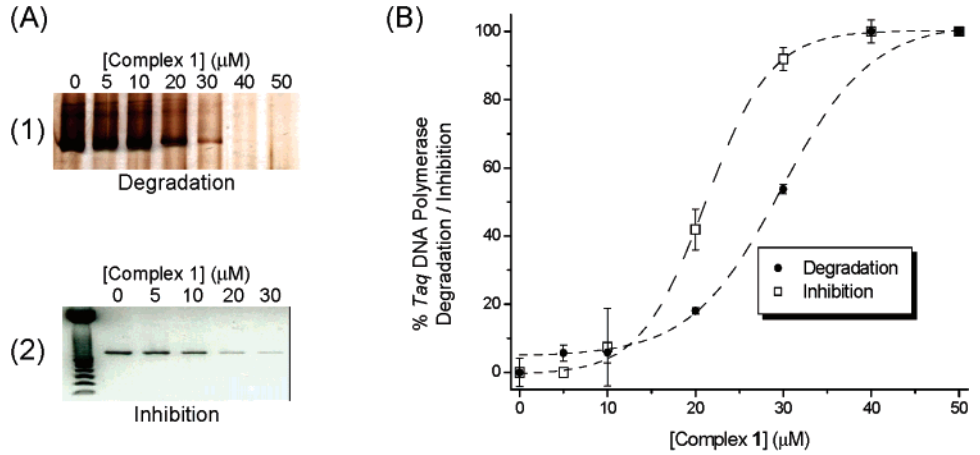

Figure 6. *Taq* DNA polymerase activity inhibition/enzyme degradation. (A_1) Purified *Taq* DNA polymerase was incubated with different complex **1** concentrations, under the same conditions as a polymerase chain reaction assay (see Experimental Section), and then submitted to electrophoresis (SDS−PAGE). (A_2) Agarose gel electrophoresis results of the 899 pb PCR product amplified by *Taq* DNA polymerase in the presence of increasing complex **1** concentrations. (B) Bands in A_1 and A_2 were quantified by densitometry and plotted against complex **1** concentration.

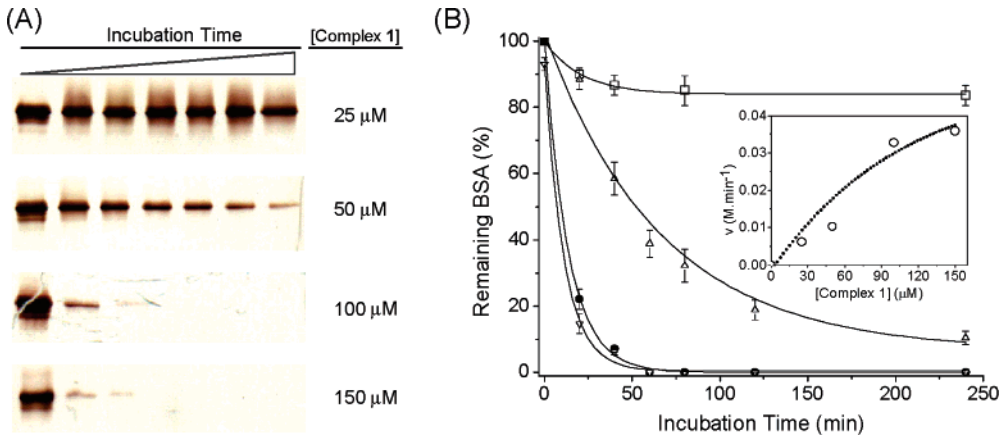

Figure 7. Time-/concentration-dependent BSA degradation: (A) SDS−PAGE of BSA (1.1 μM) incubated with different complex **1** concentrations for 0, 20, 40, 60, 80, 120, and 240 min at 70 °C, pH 8.9; (B) plot of the quantified bands in (A) against incubation time at different complex **1** concentrations (□, 25 μM; △, 50 μM; ●, 100 μM; ▽, 150 μM). The inset shows saturation kinetics of the BSA degradation (initial rates of BSA degradation versus complex **1** concentration).

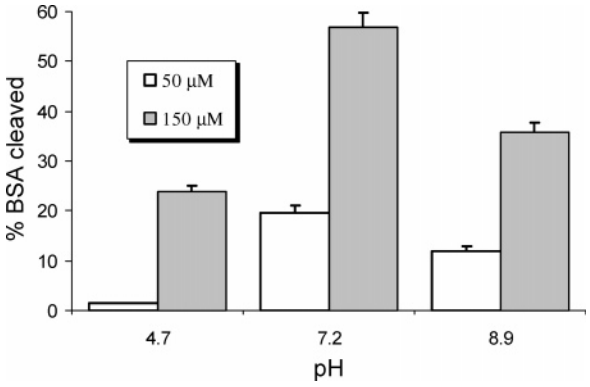

Figure 8. pH-dependent BSA degradation. BSA (1.1 μM) was degraded by 50 and 150 μM of complex **1** after 40 min of incubation at 50 °C at different pH values.

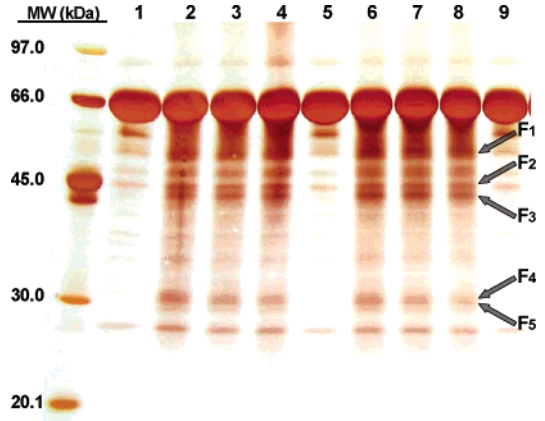

Figure 9. BSA fragmentation by complex **1** at pH 7.0 and 50 °C: lanes 1, 5, and 9, control BSA (10 μM, 240 min); lanes 2−4, BSA (10 μM) incubated with 300 μM complex **1**, for 5, 30, and 240 min, respectively; lanes 6−8, BSA (10 μM) incubated with 750 μM complex **1**, for 5, 30, and 240 min, respectively. Main cleavage products are indicated by the arrows F_1−F_5.

residues regions 1 (F205−E207), 2 (V292−D295), 3 (K362−H366), and 4 (C436−E441); the letters and numbers in parentheses refer to the amino acid position in the primary structure of BSA). It is clear that single cuts at the proposed regions 1−4 generate amino or carboxy terminal fragments of the size corresponding to that calculated by SDS−PAGE (Figure 10). A single cut in region 3, for example, generates a 41.6 kDa BSA amino-terminal fragment, which is in agreement with the observed F3 fragment in SDS−PAGE.

To further characterize the cleavage products, mass spectrometry and N-terminal sequencing of the fragaments

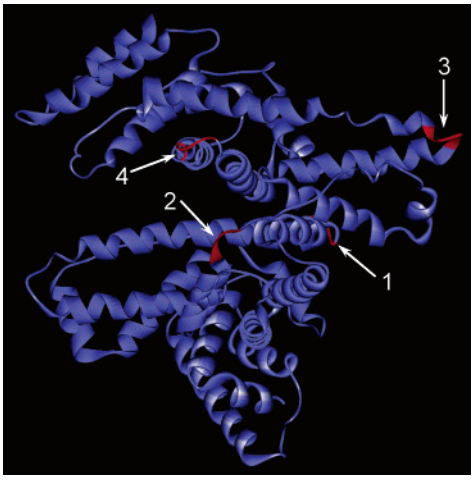

Figure 10. Three-dimensional view of BSA with the putative cleavage sites identified in Figure 5. BSA was modeled on the human serum albumin (HSA) structure (PDB 1E78) using Swiss PDB Viewer v3.7.

Table 7. Estimated Molecular Weight of BSA Fragments Generated by **1**

	frags mol wt (kDa)				
		single cut at specific region[a]			
frag	SDS−PAGE	1[b]	2	3	4
F_1	51.9				50.2 (N)
F_2	44.1	42.7 (C)[c]			
F_3	42.2			41.6 (N)	
F_4	32.6		33.7 (N)		
F_5	31.1		32.8 (C)		

[a] The molecular weights of BSA fragments were calculated with BioEdit Sequence Alignment Editor Software v 5.0.9. [b] 1−4 correspond to the putative cleavage sites promoted by complex **1** (visualized in Figure 10). [c] N and C correspond to the amino and carboxy terminal fragments, respectively.

were performed. The N-terminal is blocked in every fragment analyzed, probably due to a Schiff base formation between the N-terminal and the carbonyl group of complex **1**. A Schiff base formation between the chitosan NH_2 group and the carbonyl from complex **1** has recently been described by one of the authors.[49] Mass spectrometry results of the cleavaged products are shown in Figure S5 in the Supporting Information. As can be observed, treatment of BSA with complex **1** promoted an increase in the molecular weight of BSA. We suggest that covalent modification of lysine residues, as well as N-terminal of BSA, is occurring, as described above for the N-terminal reaction of each fragment.

Our results are also in agreement with those obtained by Burstyn[10] and Kostic,[5] for Cu([9]aneN_3)Cl_2 and Pd(II) complexes, respectively, since the cleavage sites reported for these complexes are located in close proximity to the cleavage sites suggested for complex **1** (Figures 9 and 10; Table 7).

It is important to stress the fact that the complex **1**:BSA molar ratio was in general above 10:1; thus, the kinetic parameters established here may be considered as calculated under a pseudo-Michaelis−Menten condition, with excess of catalyst over substrate as clearly depicted by Cowan for DNA cleavage agents.[50]

Anaerobic Reactions. The BSA cleavage reaction promoted by complex **1** occurred even in the presence of hydroxyradical scavengers (Figure S6), initially excluding an oxidative mechanism for BSA cleavage by complex **1**. In addition, BSA cleavage occurred in the absence of O_2 (argon atmosphere), where $[Fe(EDTA)]^{2-}$/DTT cleavage activity is highly inhibited, thus indicating a probable hydrolytic pathway inducing peptide bond cleavage. The metal(II) ion in the complex is a Lewis acid, which may bind to the carbonyl oxygen atom and render this functional group susceptible to external attack by solvent H_2O/OH^- molecules ($Cu-OH_{phenol} \leftrightarrow Cu-O_{phenolate} + H^+$; $pK_a = 5.75$) or become closer to the amide bond mediating internal attack by a coordinated $Cu-OH_2$ molecule.

Conclusions

In summary, we have synthesized and structurally characterized two new mononuclear Cu^{II} complexes with a tripodal ligand containing labile coordination sites, apparently a prerequisite in the generation of small molecules which are able to cleave important biological bonds such as P−O or C−N. As demonstrated in this study, complexes **1** and **2** are very active in peptide bond cleavage of natural substrates such as BSA and *Taq* DNA polymerase. They are active at moderate temperature (37−70 °C), and the cleavage reaction is very rapid. We estimated a half-life for the cleavage reaction of 30 min at pH 7.2. Our results suggest that complexes **1** and **2** are apparently not selective for hydrolysis of a specific peptide bond but rather for a specific region of the protein. We suggest more exposed hydrophilic regions of the protein to be the principal target.

Acknowledgment. This work was supported by grants from the CNPq, PRONEX, and PADCT. H.T. received financial support from the Third World Academy of Sciences (Grant RG BIO LA 099), CNPq of Brazil.

Supporting Information Available: Crystallographic data in CIF format and additional figures. This material is available free of charge via the Internet at http://pubs.acs.org.

IC0485864

(49) Justi, K. C.; Laranjeira, M. C. M.; Neves, A.; Mangrich, A. S.; Fávere, V. T. *Polymer* **2004**, *45*, 6285−6290.

(50) Sreedhara, A.; Freed, J. D.; Cowan, J. A. *J. Am. Chem. Soc.* **2000**, *122*, 8814−8824.